ORIGINAL ARTICLE

Study of explosive welding of A6061/SUS821L1 using interlayers with different thicknesses and the air shockwave between plates

Xiang Chen[1,2] · Xiaojie Li[3] · Daisuke Inao[4] · Shigeru Tanaka[2] · Kazuyuki Hokamoto[2] ⓘ

Abstract

In this work, SUS 304 interlayers with different thicknesses were used to weld A6061 aluminum alloy and SUS 821L1 duplex stainless steel. The effects of interlayer thickness on welding results, air shock wave between plates, and weldability window were studied. The results indicated that the interlayer thickness had a significant effect on the welding results. The shear strength of the bonding was higher than 200 MPa, when the thickness of interlayer was 0.5 mm or 0.3 mm. With the decrease of interlayer thickness, the IMCs layer became thin. When the thickness of interlayer was 0.1 mm, the welding could not be achieved, due to the unmelted A6061. The air shock wave between the plates was studied. The pressure peak of the air shock wave was calculated using "Piston model". The fluid–solid coupling finite element method was used to simulate the pressure in "Piston model" and the movement of the two different thickness interlayers (0.8 mm and 0.1 mm) under the action of the air shock wave. The simulation results indicated, with the increase of distance, the pressure peak of the air shock wave changed little, but the action time increased significantly, which improved the impulse of the air shock wave. It was proposed the influence of air shock wave should be reduced or eliminated when welding large area plates. The smoothed particle hydrodynamics (SPH) method was used to simulate the oblique impact process of the plates, and the unwelded samples were analyzed using the simulation results. In the analysis of weldability window, the influence of the interlayer on the upper and lower limits was examined, it was found that the interlayer led to an upward shift of the upper and lower limits, and the weldability window was expanded; the K value of the lower limit was obtained using numerical simulation. The collision angle between interlayer and base plate was estimated using numerical simulation.

Keywords Interlayer explosive welding · A6061/SUS821L1 · Weldability window · Air shock wave · Interlayer · SPH

1 Introduction

The joints between high-hardness aluminum alloy and stainless steel have attracted intense research interest in order to produce multi-material structures for functionalization and

✉ Kazuyuki Hokamoto
  hokamoto@mech.kumamoto-u.ac.jp

1   Hubei Province Key Laboratory of Engineering Blasting, Jianghan University, Wuhan 430056, People's Republic of China

2   Institute of Industrial Nanomaterials, Kumamoto University, Kumamoto 860-8555, Japan

3   State Key Laboratory of Structural Analysis for Industrial Equipment and Department of Engineering Mechanics, Dalian University of Technology, Dalian 116024, People's Republic of China

4   Faculty of Engineering, Kumamoto University, Kumamoto 860-8555, Japan

weight saving [1]. Currently, the main welding methods of high hardness aluminum alloy and stainless steel are friction stirring [2], TIG welding [3], and brazing [4]. These methods have limitations in practical application; for example, friction stirring limits the size of the material, while TIG welding and brazing inevitably generate an intermetallic compounds (IMCs) layer that is known to decrease the bonding strength [1].

Explosive welding is a face-to-face welding technology that can effectively control the thickness of IMCs layer [5–7]. However, in the welding of high-hardness aluminum alloy and stainless steel, a thick IMCs layer often appears at the interface, leading to welding failure [8]. To control the energy deposition at the interface, an interlayer was used to reduce the energy deposition [9]. The use of an interlayer can reduce the melting layer, enlarge the weldability window, reduce the vortex region, and reduce the large plastic deformation [10]. The interlayer such as stainless steel [9], pure

aluminum [11], low-carbon steel, or niobium [12] was used in the welding of aluminum alloy and stainless steel; high strength bonding was obtained by using various interlayers. In previous study, a SUS 821L1 interlayer was set between the flyer plate and base plate in explosive welding of high-hardness aluminum alloy (A6061) and stainless steel (SUS 821L1) [13] and 206.7 MPa shear strength was obtained. Nevertheless, a 2.5–5-μm IMCs layer was still present at the interface [13]. In this work, to obtain a thin IMCs layer at the interface, A6061 high-hardness aluminum alloy and SUS 821L1 duplex stainless steel were welded using SUS 304 thin interlayers.

The influence of air shock wave on explosive welding is rarely mentioned before. Explosive welding is usually carried out in air. For the small-size plate, the jet will quickly eject out of the gap between the flyer plate and the base plate and will not affect the welding result. However, in the welding of large plates, the air before the collision point was compressed, and the jet combustion also heated the gas in the gap, giving rise to the expansion of the gas and thus leading the flyer plate to move upward and affecting the welding results. This phenomenon is obvious in the welding of large area plate. In interlayer welding, the thickness of interlayer is thin, the effect of air shock wave will more obvious. In this work, the air shockwave between the plates was studied by theoretical analysis and simulations. It is the first time to use numerical simulation to study the air shock wave between explosive welding plates. The evolution of air shock wave between plates was analyzed, and the influence of air shock wave on the movement of interlayer was obtained.

Weldability window is used to guide the selection of welding parameters. We analyzed how the interlayer expands the upper limit in the previous work [13]. No quantitative analysis has been done about the influence of interlayer on the lower limit yet. In this work, the effect of the interlayer thickness on the weldability window was examined using smoothed particle hydrodynamics (SPH) simulations. Through numerical simulation, the K values of the lower limits for direct welding and interlayer welding were given.

2 Materials and methods

The schematic of interlayer explosive welding is shown in Fig. 1. β_1 is the collision angle between flyer plate and interlayer; β_2 is the collision angle between interlayer and base plate. Five-millimeter-thick JIS A6061 was used as the flyer plate, and 3-mm-thick JIS SUS 821L1 was used as the base plate [17]. To keep the materials of the interlayer and base plate same, a thin SUS 821L1 plate was required. However, no commercial 0.1~0.5 mm SUS 821L1 plate can be purchased. To keep the material of interlayer and base plate similar, due to the density and composition of SUS 304 were similar to SUS 821L1, the 0.5-mm-thick, 0.3-mm-thick, and 0.1-mm-thick JIS SUS 304 were used as the interlayer. The chemical and mechanical properties of materials are shown in Tables 1 and 2. The Vickers hardness was measured using Vickers hardness tester (HM-200, Mitutoyo). The hardness of different surfaces of SUS 821L1 varies greatly as shown in Table 2. The size of the plates is 200×100 mm (length×width). An anvil was set under the base plate. The size of the anvil is 260×140×60 mm

Fig. 1 Schematic of explosive welding with an interlayer
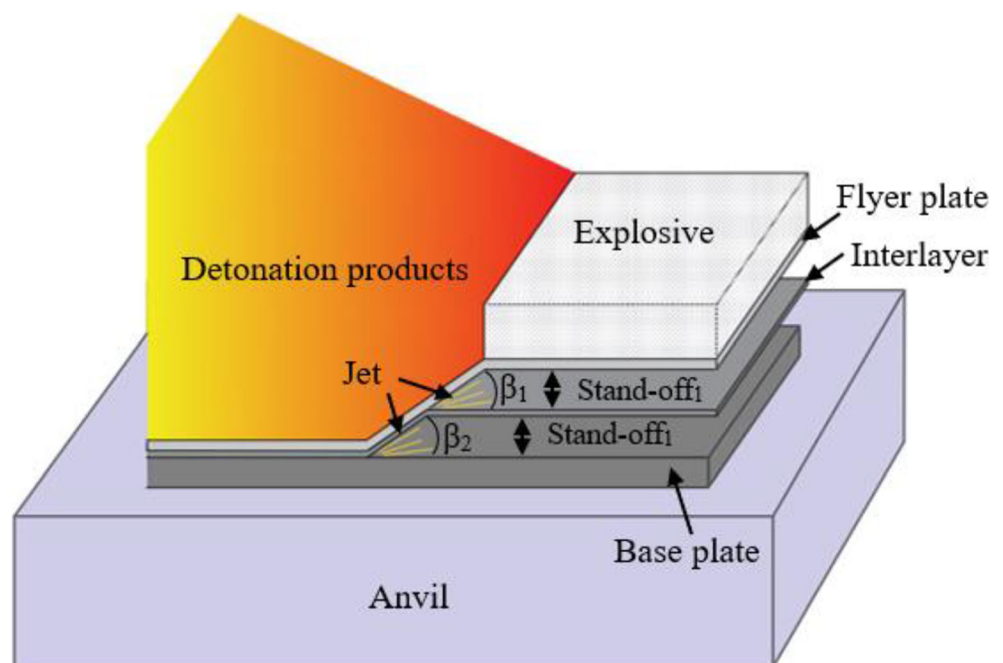
Table 1 Chemical composition of the materials (mass pct)

	Si	Fe	Cu	Mg	Cr	Al
A6061	0.40~0.80	<0.70	0.15~0.40	0.80~1.20	0.04~0.35	bal.
	Si	C	Mn	Ni	Cr	Fe
SUS 304	≤1.00	≤0.08	≤2.00	8.00~10.50	18.00~20.00	bal.
SUS 821L1	≤0.75	≤0.03	2.0~4.0	1.50~2.50	20.50~21.50	bal.

(length×width×height). At each corn of the plate, a 5×5×2-mm (length×width×height) stand-off was set to keep the distance between the plates. The stand-off is made by PMMA. The explosive used in the experiment was ANFO-A (a mixture of ammonium nitrate and fuel oil) with a density of about 530 kg/m^3. The thickness and detonation velocity of the explosive are given in Table 3. The values of the K and V_D in Table 3 can be found in the references [9, 18].

Flyer plate velocity (V_P) and the collision angle (β) are important factors for the calculation of the welding parameters of explosives. The relationship can be expressed using the following equation [19]:

$$V_P = 2V_D \sin\frac{\beta}{2} \tag{1}$$

where V_D is the detonation velocity of the explosive. The collision angle β can be calculated using the following equation [20]:

$$\beta = \left(\sqrt{\frac{K+1}{K-1}}-1\right)\frac{\pi}{2}\frac{r}{r+2.71+\frac{0.184t_e}{s}} \tag{2}$$

where r is the loading ratio (mass of explosive per unit mass of flyer plate), t_e and s are the explosive thickness and the stand-off distance, respectively, and K is the gaseous polytropic index of the detonation products.

The energy dissipated at the interface during the collision has an important effect on the results of explosive welding. In direct explosive welding, the kinetic energy loss (ΔKE) during the collision can be obtained using the following equation [9]:

$$\Delta KE = \frac{\left(m_D m_C V_P^2\right)}{2\left(m_D + m_C\right)} \tag{3}$$

where m_C is the mass per unit area of the collided plate, and m_D is the mass per unit area of the flyer plate. Equation (3) shows reducing the mass of flyer plate, or collide plate can reduce the kinetic energy loss; the kinetic energy loss is positively correlated with the energy deposited on the interface. The energy deposited on the interface can be controlled by only changing the thickness of interlayer. Table 4 shows the kinetic energy loss at the interface using different thickness of interlayer. Using the method in the reference [13] to calculate the two boundaries of the flyer plate velocity in interlayer welding, the calculated results are presented in Table 4. ΔKE_1 is the kinetic energy loss between the flyer plate and the interlayer; it was calculated using V_{Pmin}.

3 Results and discussions

3.1 Morphology of the interface

The prepared samples were analyzed using an optical microscope (Measurescope UM-2, Nikon) and a scanning electron microscope (JCM-5700, JEOL Ltd) as shown in Fig. 2. Figure 2 shows the morphology of the interface obtained using different welding conditions. It is observed that samples 1, 4, and 5 were not welded. For sample 1, this may be due to the excessive energy deposition at the interface; while for samples 4 and 5, this may be due to the low energy deposition at the interface. Below, we will analyze the origin for the lack of welding of samples 1, 4, and 5 by combining simulation results and the weldability window. Due to the melting of aluminum alloy during the collision, melting and atom diffusion occurred between aluminum alloy and SUS 304; the alloy phases between explosive welded aluminum alloy and stainless steel were analyzed in previous work [13]; the main

Table 2 Mechanical properties [14–16]

	Density (g/cm^3)	Yield strength (N/mm^2)	Tensile strength (N/mm^2)	Elongation (%)	Hardness of welding surface (HV)	Hardness of thickness surface (HV)
A6061	2.71	≥276	≥310	-	108	108
SUS 304	7.90	≥205	≥520	≥40	380	380
SUS 821L1	7.80	≥400	≥600	≥25	245	300

Table 3 Experimental parameters and results

Samples	K	Thickness of explosive (mm)	Detonation velocity D (m/s)	Stand-off$_1$ (mm)	Stand-off$_2$ (mm)	Interlayer	Welding results
1	2.37	38	2450	2	/	/	Unwelded
2	2.48	48	2575	2	2	0.5-mm SUS 304	Welded
3	2.48	48	2575	2	2	0.3-mm SUS 304	Welded
4	2.48	48	2575	2	2	0.1-mm SUS 304	Unwelded
5	2.20	28	2350	2	2	0.1-mm SUS 304	Unwelded

components of the IMCs were Al and Fe_4Al_{13}. The IMCs layer of sample 2 was 1–5 μm, and the IMCs layer always existed at the interface. The IMCs layer of sample 3 was 0–2 μm. At a magnification of ×2000 under SEM, the IMCs layer of sample 3 was difficult to observe; the sub-micron atomic diffusion had happened at the interface. Comparison of samples 2 and 3 clearly showed that a thinner interlayer led to the lesser formation of IMCs. The interface between the aluminum alloy and interlayer was nearly flat, indicating that the welding parameters were at the left side of the weldability window's left limit. The interface between the interlayer and base plate of sample 4 is wavy, while that of sample 5 is flat, implying that the weldability window's left limit for SUS 304 and SUS 821L1 is between 2350 and 2575 m/s.

3.2 Mechanical properties

3.2.1 Tensile shear test

The samples were processed using the method described in a previous work [13]; the fracture appeared on the A6061 side in the previous work; it might be due to the axis of the force is on the A6061 side. In this experiment, to ensure the axis of the force is near the interface, the aluminum alloy side was machined to a thickness of 3 mm. The schematic of the tensile test sample is shown in Fig. 3a. A universal testing machine (AG-250kNXplus, Shimadzu) was used in the test. In Table 5, the measured shear strengths of the two samples

were almost the same, and the samples differed mainly in regard to the fracture location. As shown in Fig. 3, the fracture of sample 2 appeared on the A6061 side, indicating that the bonding at the interface was higher than the measured value, while the fracture of sample 3 appeared at the interface, suggesting that the measured value was the bonding strength of the interface. The relatively low bonding strength of sample 3 may be due to the thin IMCs layer at the interface. Although a too thick melting layer is known to have a negative effect on the welding strength, the present experimental results showed that a certain thickness of the melting layer is beneficial for welding strength.

3.2.2 Vickers hardness test

The results of Vickers hardness tests are shown in Fig. 4. A loading of 0.2 kgf was used to measure the hardness of SUS 304 and SUS 821L1, and a loading of 0.05 kgf was used to measure the hardness of A6061. Work hardening often appears in explosive welded metals. Compared with the hardness before and after explosive welding, the Vickers hardness of A6061 did not change much. Carvalho et al. mentioned that work hardening was not an effective hardening mechanism for Al alloys [8]; we thought it might also be related to the small plastic deformation on the A6061 side. The deformation of SUS 304 and SUS 821L1 is large; the work hardening of them is obvious as shown in Fig. 4 b and d.

Table 4 Calculated V_P, β, and ΔKE

Sample	K	Detonation velocity (m/s)	Explosive ratio r	Velocity of flying plate V_{Pmin} (m/s)	Velocity of flying plate V_{Pmax} (m/s)	Collision angle β_{min}	Collision angle β_{max}	ΔKE_1 (KJ/m²)
1	2.37	2450	1.49	423	/	9.9°	/	1177
2	2.48	2575	1.88	450	596	10.0°	13.3°	310
3	2.48	2575	1.88	450	596	10.0°	13.3°	205
4	2.48	2575	1.88	450	596	10.0°	13.3°	76
5	2.20	2350	1.10	402	502	9.8°	12.3°	60

Fig. 2 Optical analysis and SEM
analysis of the interface: **a**, **b**
sample 1; **c**, **d e** sample 2; **f**, **g**, **h**, **i**
sample 3; **j**, **k** sample 4; **l**, **m**
sample 5
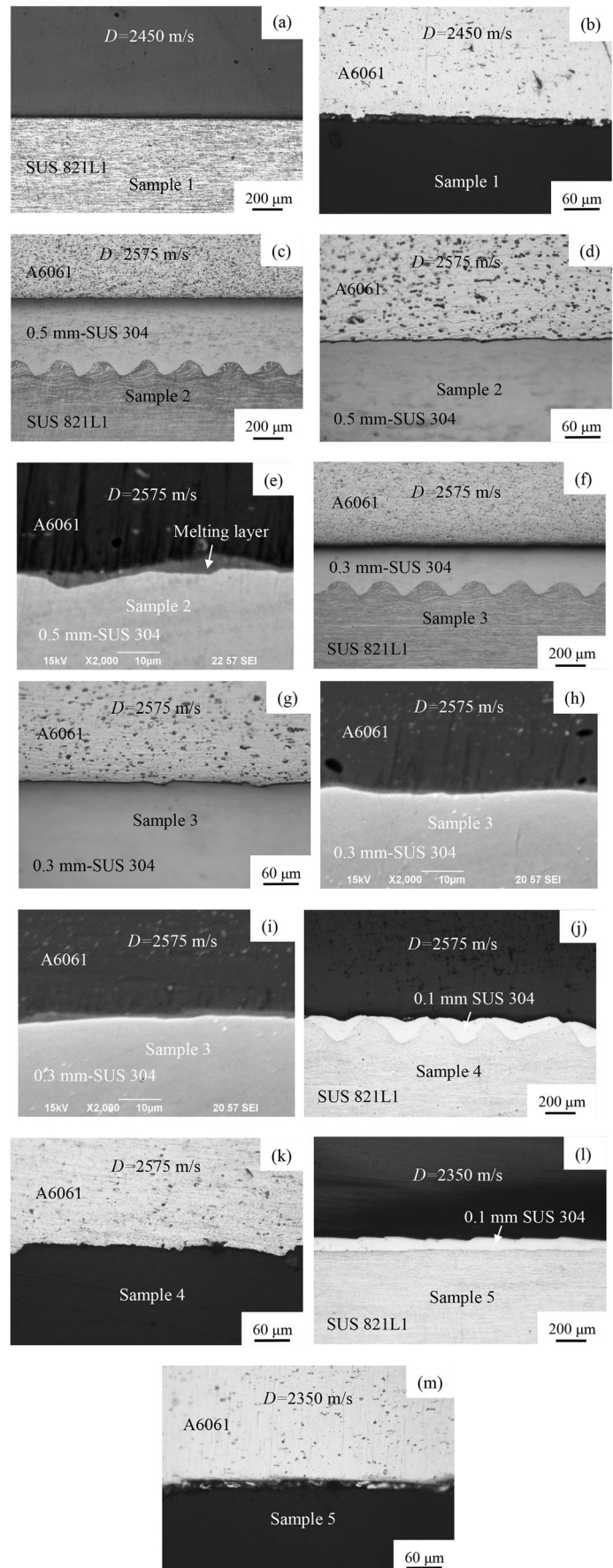
Fig. 3 Tensile shear test: **a** schematic of tensile test sample; **b** tensile shear curve; **c** and **d** fracture of sample 2; **e** and **f** fracture of sample 3
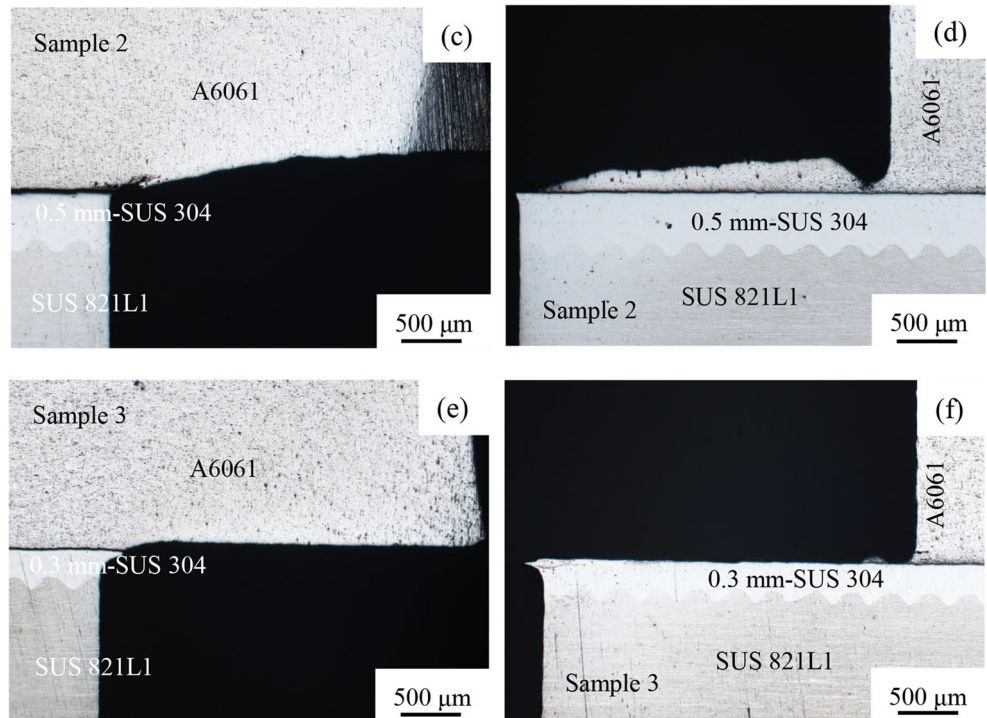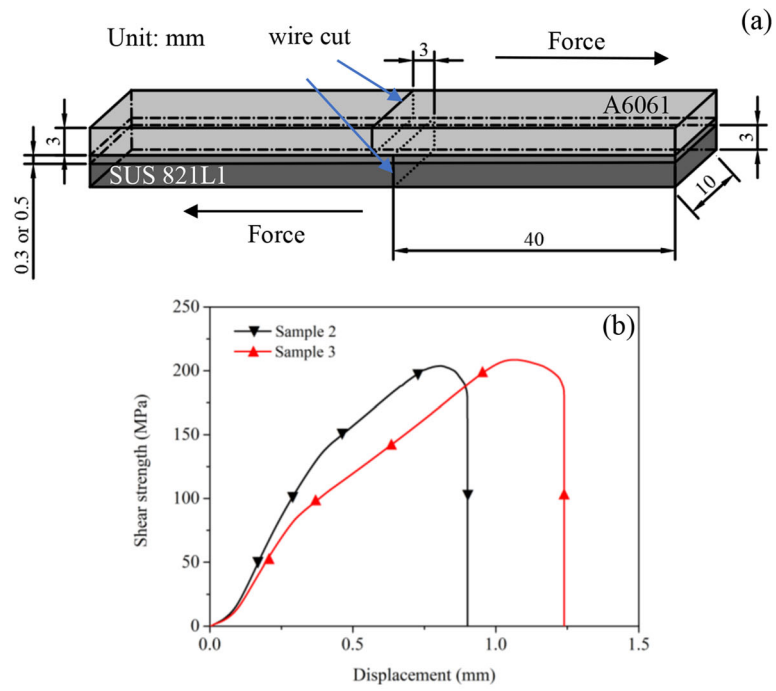
Table 5 Tensile shear test parameters

Sample	Length×width×height (mm)	Actual distance between cuts (mm)	Loading speed (mm/min)	Measured shear strength (MPa)	Main location of fracture
2	83.10×9.72×5.80	2.73	0.1	203.8	A6061 side
3	83.00×10.00×5.80	2.73	0.1	208.6	Interface
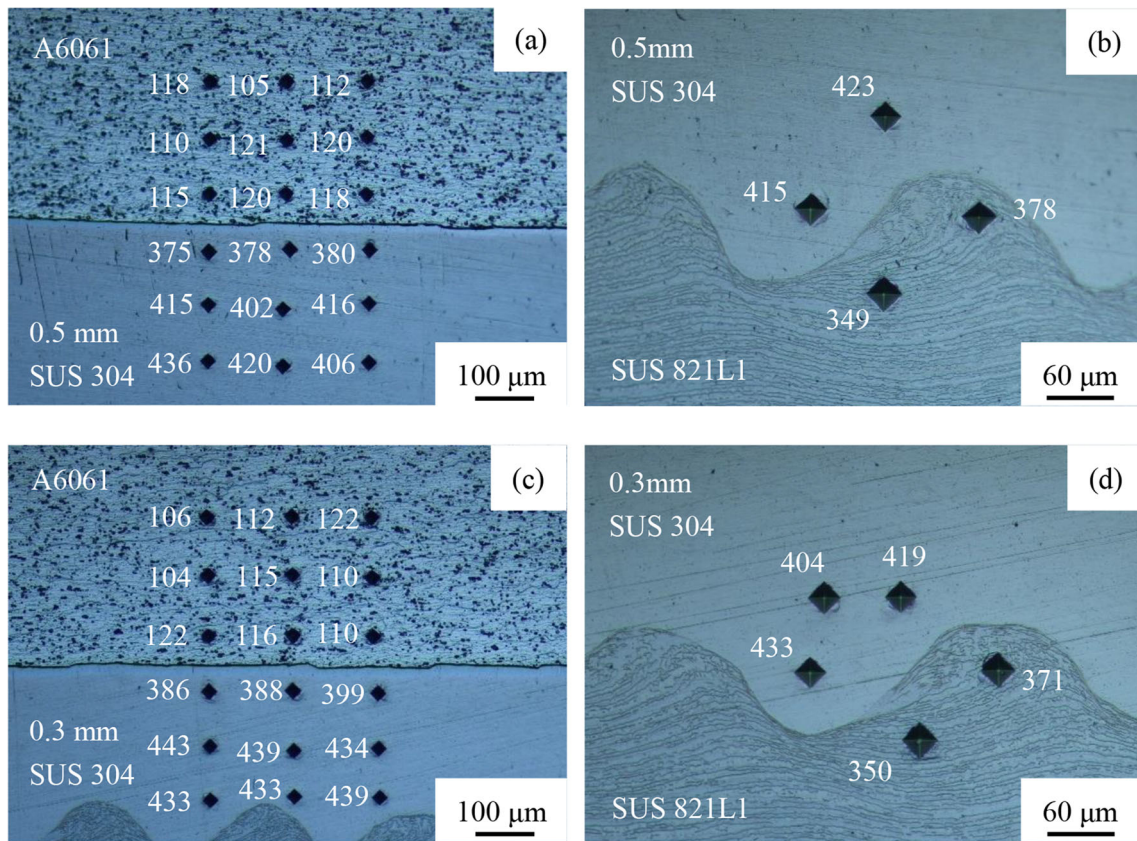
Fig. 4 Vickers hardness: **a** interface between A6061 and 0.5-mm SUS 304; **b** interface between 0.5-mm SUS 304 and SUS 821L1; **c** interface between A6061 and 0.3-mm SUS 304; **d** interface between 0.3-mm SUS 304 and SUS 821L1

4 The air shock wave between plates

4.1 Theoretical analysis

In interlayer welding, the interlayer is usually thin. In this part, we want to study the influence of air shock wave on the interlayer explosive welding process. Explosive welding is usually carried out in air. For the small size plate, the jet will quickly eject out of the gap between the flyer plate and the base plate and will not affect the welding result. However, in the welding of large plates, the air before the collision point was compressed, and the jet combustion also heated the gas in the gap, giving rise to the expansion of the gas and thus leading the flyer plate to move upward and affecting the welding results.

When the collision point between the flyer plate and the base plate moves from left to right, it acts as a moving "piston" and compresses the gas in the gap, as shown in Fig. 5a, and its speed is equal to the detonation velocity V_d. A gas shockwave will form in the gap. The air shockwave between the flyer plate and interlayer will propagate ahead of the detonation wave as shown in Fig. 5b, so that the flyer plate will be jacked up and the density of the explosive on the flyer plate will change. These phenomena will change the welding parameters, affecting the welding result. Assuming that the velocity

of air shockwave is D, the gas in front of the air shockwave is the undisturbed area, the gas velocity is 0, the pressure is atmospheric pressure P_0, the gas density is ρ_0, the internal energy per unit mass is E_0, the sound velocity is C_0, and the corresponding parameters after the impact of the shockwave are V_d, P, ρ, E, and C, then the parameters satisfy the following shockwave relations in the piston model:
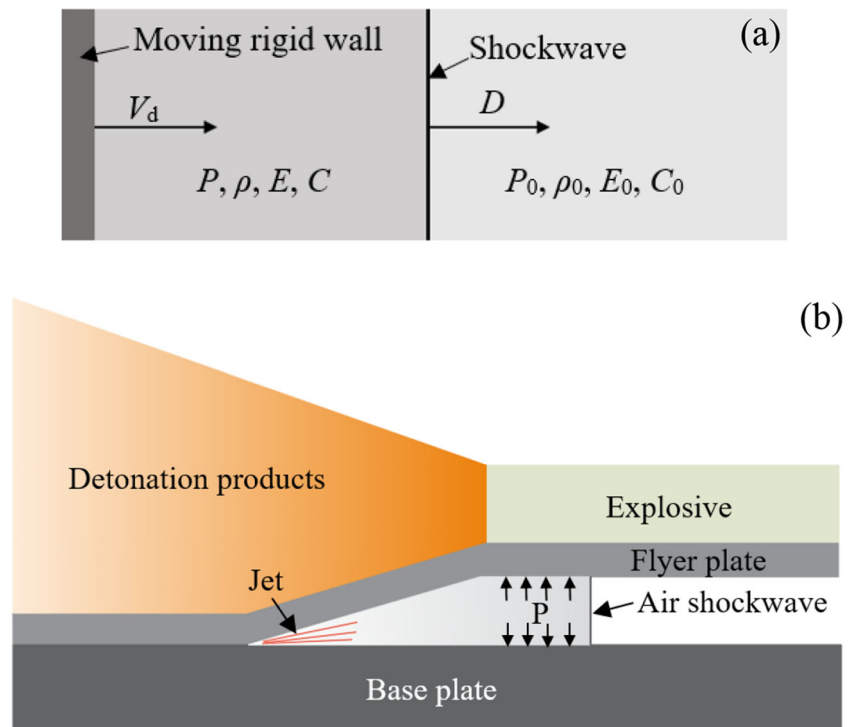
$$
\begin{cases}
\rho_0 D = \rho(D - V_d) \\
P - P_0 = \rho_0 D V_d \\
E - E_0 = \dfrac{1}{2}(P + P_0)\left(\dfrac{1}{\rho_0} - \dfrac{1}{\rho}\right)
\end{cases}
\tag{4}
$$

The specific internal energy E and sound velocity C can be obtained by using the polytropic gas equation.

$$
E = \frac{1}{\gamma - 1}\frac{P}{\rho}; \quad C = \sqrt{\frac{\gamma P}{\rho}}
\tag{5}
$$

where γ is the adiabatic exponent. In Eq. (4), the parameters for the gas in front of the shockwave are known, and the particle velocity after the shockwave is V_d, and the parameters of interest are the shockwave velocity D and shockwave pressure P. The E of Eq. (5) is substituted into Eq. (4) to obtain:

$$
\begin{cases}
\dfrac{\rho_0}{\rho} = 1 - \dfrac{V_d}{D} \\[2mm]
P = P_0 + \rho_0 D V_d \\[2mm]
\dfrac{2\rho_0 \left(\dfrac{P}{\rho} - \dfrac{P_0}{\rho_0} \right)}{\gamma - 1} = \dfrac{P + P_0}{1 - \dfrac{\rho_0}{\rho}}
\end{cases}
\tag{6}
$$

By combining Eqs. (5) and (6), the following one variable quadratic algebraic equation in D can be obtained:

$$
\left(\frac{D}{V_d} \right)^2 - \frac{\gamma + 1}{2} \left(\frac{D}{V_d} \right) - \left(\frac{C_0}{V_d} \right)^2 = 0
\tag{7}
$$

$$
\begin{cases}
\dfrac{D}{V_d} = \dfrac{\gamma + 1}{4} \pm \sqrt{\dfrac{(\gamma + 1)^2}{16} + \left(\dfrac{C_0}{V_d} \right)^2} \\[2mm]
P - P_0 = \rho_0 D V_d
\end{cases}
\tag{8}
$$

The pressure of the gas between the flyer plate and base plate can be obtained by Eq. (8). The actual situation is much more complex than the above model; for example, the gas does not satisfy the ideal gas hypothesis, and the high temperature and pressure of the shockwave will ionize the gas [21, 22] decreasing the adiabatic exponent and the shockwave velocity and pressure. However, the jet will enter the high temperature and high pressure air shockwave. The metal particles in the jet react with oxygen, nitrogen, and other gases in the air shockwave, changing the gas composition and increasing its internal energy and mass density, thus increasing the shockwave pressure. In addition, the high pressure generated by the

shockwave will squeeze and lift the clad plate and explosive, increase the space after the shockwave, and decrease the pressure. Considering these factors, it is clear that accurate results cannot be obtained by Eq. (8); nevertheless, the model of Eq. (8) can still roughly reflect the gas flow between the flyer plate and base plate. As mentioned above, the air shock phenomenon will be obvious in the welding of large plates.

In interlayer welding, the interlayer is usually thin. Under the action of the air shockwaves between the flyer plate and interlayer, and between the interlayer and the base plate, the interlayer will swing. In the schematic of the air shock wave in interlayer shown in Fig. 6, due to welding time is very short, the movement of the interlayer under gravity is ignored. The parameters of the air are listed in Table 6. The calculation results using the piston model are shown in Table 7, and it is observed the air shock wave becomes stronger with increasing detonation velocity. Since realistic interlayer explosive welding is different from the piston model, the air shock wave between the plates was studied by numerical simulations.

4.2 Simulation of shock wave between plates

4.2.1 Piston model

To test the reliability of the numerical simulation, the piston model was simulated at first. The fluid–solid coupling finite element algorithm was used to simulate the piston model. Air used the Euler algorithm; rigid wall used the Lagrange algorithm. The right boundary of air was flowing out boundary,

Fig. 6 Schematic of the air shock wave during interlayer explosive welding
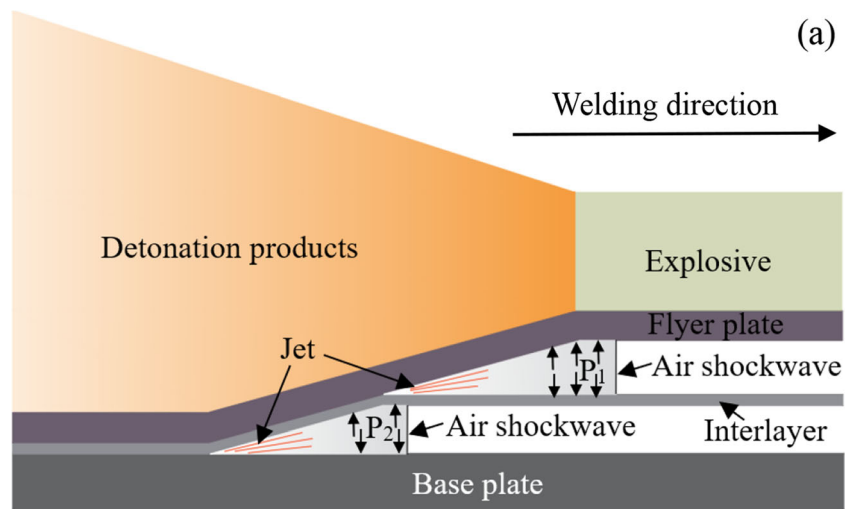
and other boundaries of air were fixed boundaries. The velocity of the rigid wall was 2575 m/s and 2450 m/s, respectively. The numerical model is shown in Fig. 7a, and 9 observation points were set up. Figure 7b indicates that the pressure was uniform in front of the moving rigid wall, and the action time of the shock wave increased according to the distance as shown in Fig. 7c. The obtained simulated results presented in Table 8 are close to the calculated results presented in Table 7, verifying the accuracy of the numerical simulations.

4.2.2 Simulation of shock wave in interlayer explosive welding

The parameters used in the simulation are shown in Tables 9 and 10, and the parameters of the ANFO explosive used the modified JWL equation in reference [26]. Air and ANFO used the Euler algorithm; A6061, interlayer, SUS 821L1, and steel 1006 used the Lagrange algorithm. All the boundaries of the air used flowing out boundaries. The thickness of the interlayer using in simulation was 0.1 mm and 0.8 mm, respectively. The numerical model is shown in Fig. 8a. The pressure between the flyer plate and interlayer was smaller than the pressure between the interlayer and the base plate as shown in Fig. 8b. Similar to the piston model, the action time of the shock wave was found to increase with the distance as shown in Fig. 8 c and h. The impulse of the air shock wave in Fig. 8 d and i increases the distance, implying that the impact of the air shock wave will be greater farther

away from the initiation point. Figure 8 e and j show that the interlayer had a non-zero velocity under the air shock wave. The displacement caused by the velocity is shown in Fig. 8 f and k, and it is observed that the displacement of the 0.1-mm-thick interlayer was greater than that of the 0.8-mm-thick interlayer. Figure 8 g and l indicated that the air shock wave caused the plastic deformation of the plate. The pressure distribution of the air shock wave is shown in Fig. 8 m and n, and it is observed that with the increase in the propagation distance of the air shock wave, the distance S between the two air shock waves decreased due to the interlayer movement downward under the action of the air shock wave between the flyer plate and the interlayer. This movement expanded the space between the flyer plate and interlayer, and weakened the shock wave between the flyer plate and the interlayer. At the same time, the movement reduced the space between the interlayer and the base plate and strengthened the shock wave between the interlayer and the base plate. If the length of the plate is large enough, the shock wave between the interlayer and the base plate will catch up with the shock wave between the flyer plate and the interlayer. In this case, the interlayer will move upward, the shock wave between interlayer and base plate will be weakened, and the shock wave between the flyer plate and the interlayer will be strengthened, causing the whole interlayer to swing up and down. The simulation results show that the effect of the air shock wave is more pronounced for thinner interlayers.

Table 6 Parameters of air

Molecular weight M	Adiabatic exponent γ	Sound velocity at atmospheric pressure C_0 (m/s)	Density ρ (kg/m³)
28.959	1.404	331	1.292

Table 7 Pressure of the air shockwave calculated by the piston model

Sample	Detonation velocity (m/s)	D/V_d	Air shockwave P (MPa)
4	2575	1.216	10.417
5	2350	1.218	8.676

Fig. 7 Simulation of the air shock wave using the piston model: **a** numerical model; **b** pressure distribution; **c** pressure curve of points 4, 5, and 6 of the oblique collision model
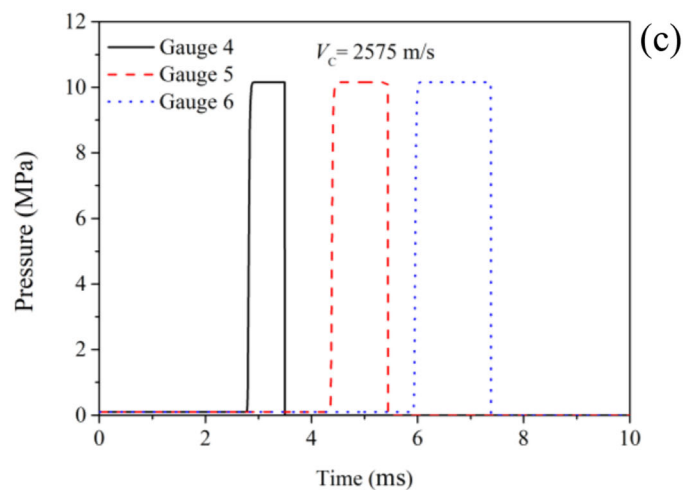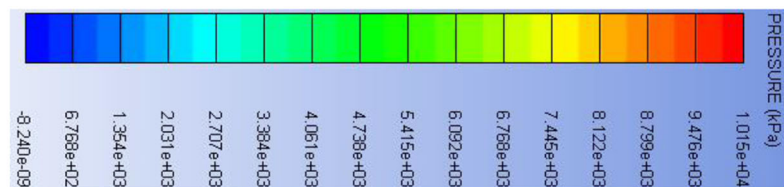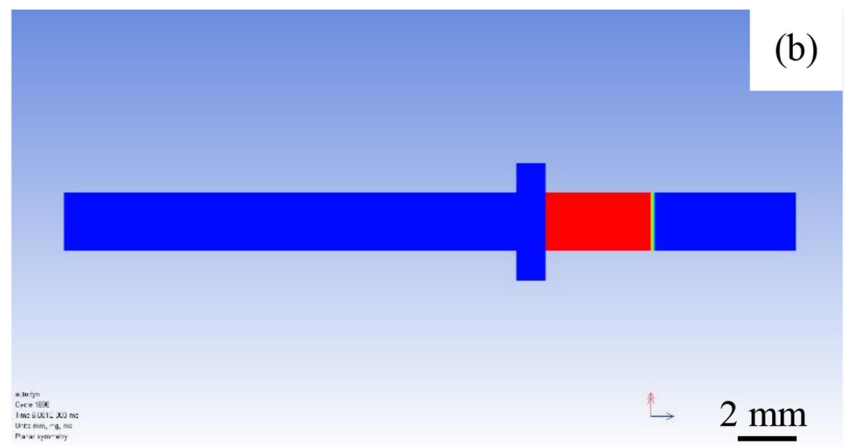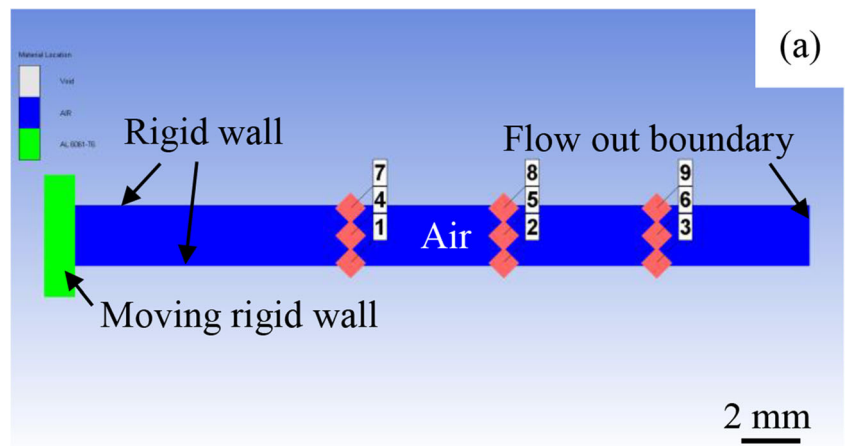
Table 8 Peak pressure of the observation point (unit: MPa)

	Gauge 1	Gauge 2	Gauge 3	Gauge 4	Gauge 5	Gauge 6	Gauge 7	Gauge 8	Gauge 9
Piston model									
2575 m/s	10.15	10.15	10.15	10.15	10.15	10.15	10.15	10.15	10.15
2350 m/s	8.48	8.48	8.48	8.48	8.48	8.48	8.48	8.48	8.48

5 Numerical simulation of welding process

The SPH numerical method is suitable for simulating large deformations and has been extensively used for the simulations of explosive welding processes. In particular, the simulations of the explosive welding process have been performed using the inclined collision of plates at a given flyer plate velocity V_P and collision angle β [27, 28]. The numerical model is shown in Fig. 9a.

The collision angle between flyer plate and interlayer can be calculated by Eq. (2). However, the collision angle between interlayer and base plate is difficult to obtain. We proposed a method in previous work [13] to estimate the collision angle between interlayer and base plate. The calculated parameters under the two boundary conditions are shown in Table 4. The parameters of V_{Pmin} and β_{min} were used in the simulation of the flyer plate and the interlayer, and the parameters V_{Pmax} and β_{max} were used in the simulation of the interlayer and the base plate. The simulated collision angle between the interlayer and the base plate are shown in Table 11.

The Von Mises stress was used to evaluate the melting [29]. The simulated results presented in Fig. 9 show that the jet was propagating only from the A6061 side. The jet and melting were reduced with decreasing thickness of the collided plate. No jet or melting was observed when using the 0.1-mm-thick interlayer. The simulation results indicated that sample 1 was not welded due to the high-energy deposition at the interface, and the excessive melting led to the welding failure. Samples 4 and 5 were not welded due to the low energy deposition at the interface, and no jet and melting appeared at the interface of samples 4 and 5. The wave between the interface and the base plate increased with

decreasing thickness of the interlayer. The jet in Fig. 9n may penetrate the interlayer, and then form the irregular interface as shown in Fig. 9p.

6 Weldability windows

Weldability window is often used to guide the parameters selection in explosive welding. The lower limit and upper limit of the window are related to the energy deposition on the interface. The lower limit is related to the jet; when the energy deposition at the interface decreases, the jet process will become difficult; to generate the jet, under the same detonation velocity, the collision angel needs to increase, so the lower limit will move upward. The upper limit is related to excessive melting; when the energy deposition at the interface decreases, the melting will decrease; the upper limit will move upward. The weldability windows in Fig. 10 were constructed using the method in reference [13] and the parameters in Table 12, and the lower limit was obtained by numerical simulations. The left limit in reference [13] was used as the original data for A1100 and A6061 in the work of Cowan et al. [31], whereas in this work the average value of the Reynolds number R_T =10.6 was used in the left limit calculation of A6061 and stainless steels, the Reynolds number of SUS 304 and SUS 821L1 was estimated using the experimental result. The right limit was used based on the method proposed by De Rosset [32]. Due to the low melting point of A6061, the upper limit is stricter [13], and N=0.15 was used in the upper limit calculation. For different interlayers, in the upper limit calculation, the N values were determined using the ratio of the deposition energy to direct welding, and the upper limit used for SUS 304/SUS 821L1 was N=0.037 [13]. Figure 10a shows that the welding parameters of sample 1 are near the

Table 9 Parameters of the shock equation of state [23]

Materials	Gruneisen coefficient γ	Parameter C_1 (m/s)	Parameter S_1	Reference temperature (K)	Specific heat (J·kg^{-1}·K^{-1})
A6061	1.97	5240	1.40	300	885
SUS 821L1	2.17	4569	1.49	300	452
SUS 304	2.17	4569	1.49	300	452
Steel 1006	2.17	4569	1.49	300	452

Table 10 Johnson–Cook's law parameters [24, 25]

	A (MPa)	B (MPa)	C	n	m	T_m
A6061	324	114	0.002	0.42	1.34	855 K
SUS 821L1	577	1100	0.015	0.50	0.70	1811 K
SUS 304	280	1100	0.015	0.50	0.70	1811 K
STEEL 1006	350	275	0.022	0.36	1.00	1811 K
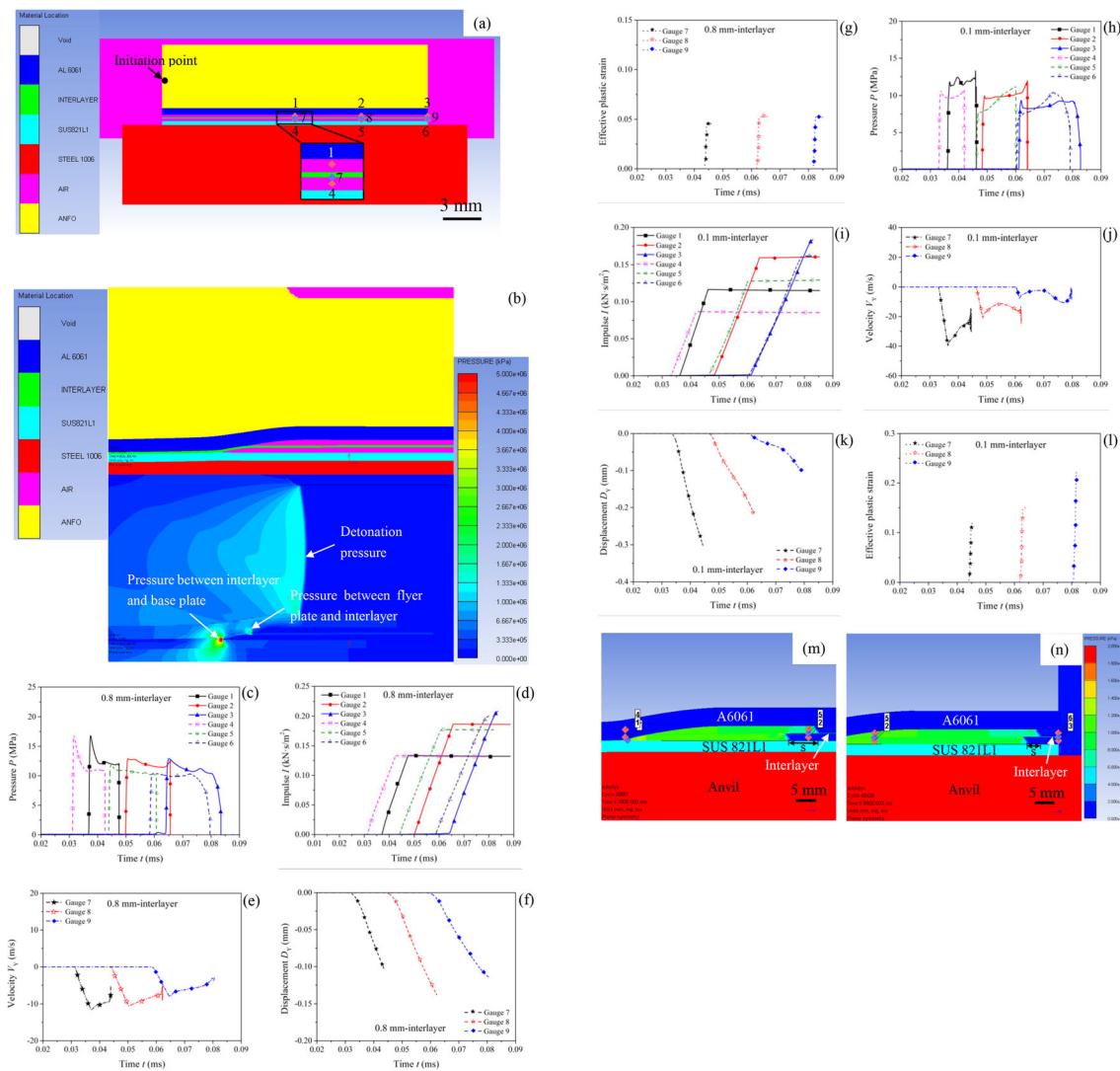
Fig. 8 Simulation of the air shock wave between the plates: **a** numerical model; **b** pressure distribution of the 0.8-mm-thick interlayer explosive welding; **c**, **h** pressure of the air shock wave; **d**, **i** impulse of the air shock wave; **e**, **j** interlayer's velocity under the air shock wave; **f**, **k** interlayer's displacement under air shock; **g**, **l** effective plastic strain under the air shock wave; **m**, **n** pressure distribution of the 0.1-mm-thick interlayer

upper limit, suggesting that excessive melting caused the welding failure, in agreement with the simulation analysis. The upper limit was expanded upward by using the interlayer as shown in Fig. 10b, so that the welding was facilitate by using the interlayers. Figure 10c indicates that it was more difficult to produce the jet for thinner interlayers. The parameters of samples 4 and 5 were below the lower limit, so that no jet was generated between the flyer plate and the interlayer during the collision process, leading to the failure of welding. Figure 10d shows that although when using an interlayer, the lower limit and upper limit both shift upward, and the area of the window was expanded. Due to the use of the average value of the Reynolds number, the calculated left limits were not accurate, and according to the experimental results, the welding parameters were at the left side of the left limits. The weldability window between interlayer and base plate is shown in Fig. 10e. From the experimental results in Fig. 2 j

and l, it can deduce the R_T of SUS 304/SUS 821L1 is between 6.9 and 8.3.

7 Conclusions

1. For explosive welding of A6061 and SUS 821L1, too much or too little energy deposited on the interface leads to welding failure. Three different thicknesses SUS 304 (0.5 mm, 0.3 mm, 0.1 mm) were used as the interlayer to control the energy deposited on the interface between flyer and interlayer. The results indicated the energy deposition on the interface affected the thickness of the melting layer and the bonding strength. When the thickness of the interlayer was 0.5 mm, the thickness of IMCs was 1–5 µm; the shear strength between A6061 and interlayer was higher than 203.8 MPa; the fracture appeared on A6061

Fig. 9 Simulation of oblique collision: **a** numerical model; **b**–**f** the jet and interface between flyer plate and collided plate; **g**–**k** the melting (Von Mises stress=0) between the flyer plate and the collided plate (blue area is the melting area); **l**–**o** the jet between the interlayer and the base plate; **p** irregular interface of sample 4
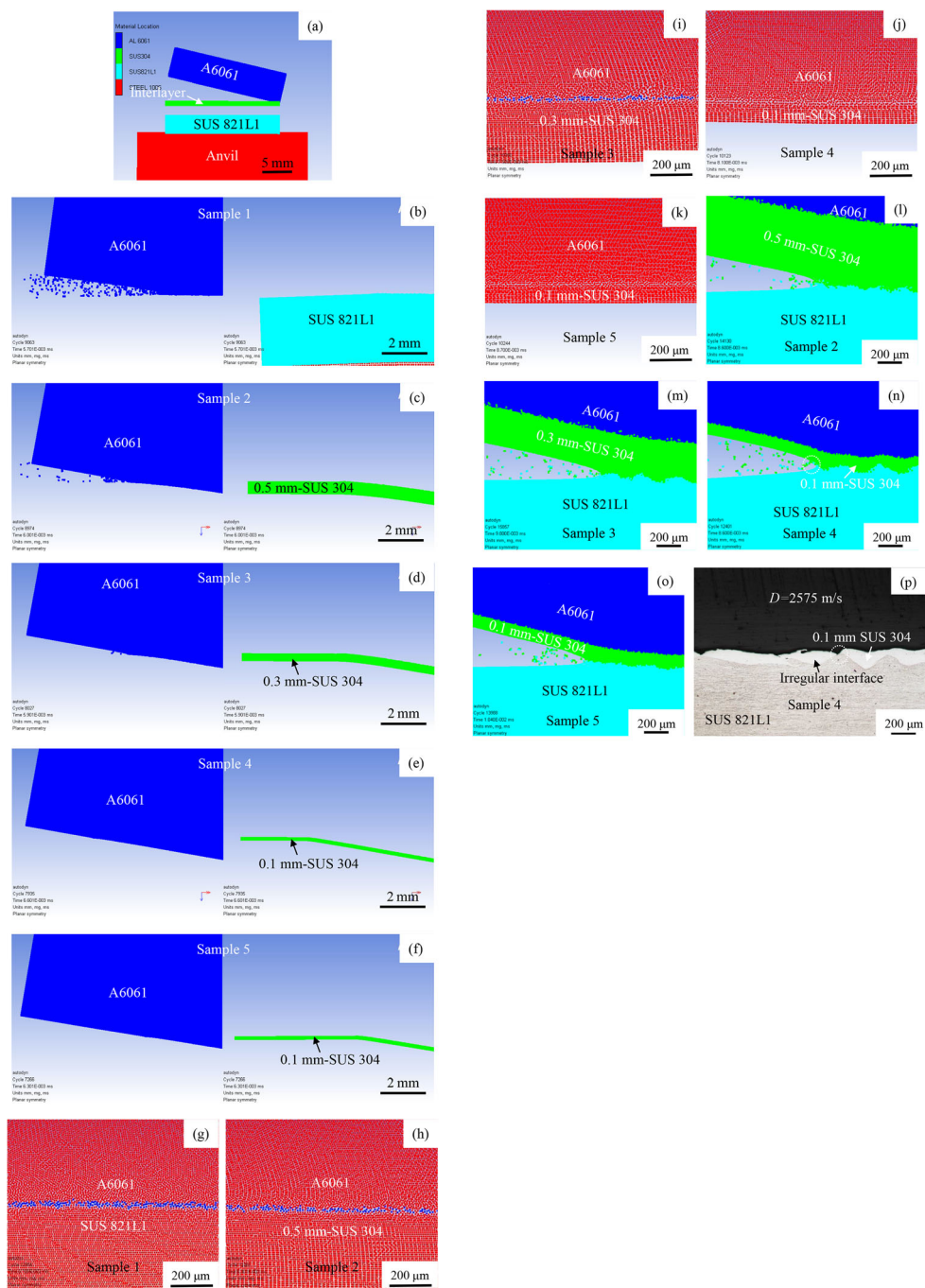
side. When the thickness of the interlayer was 0.3 mm, the thickness of IMCs was 0–2 μm, the shear strength

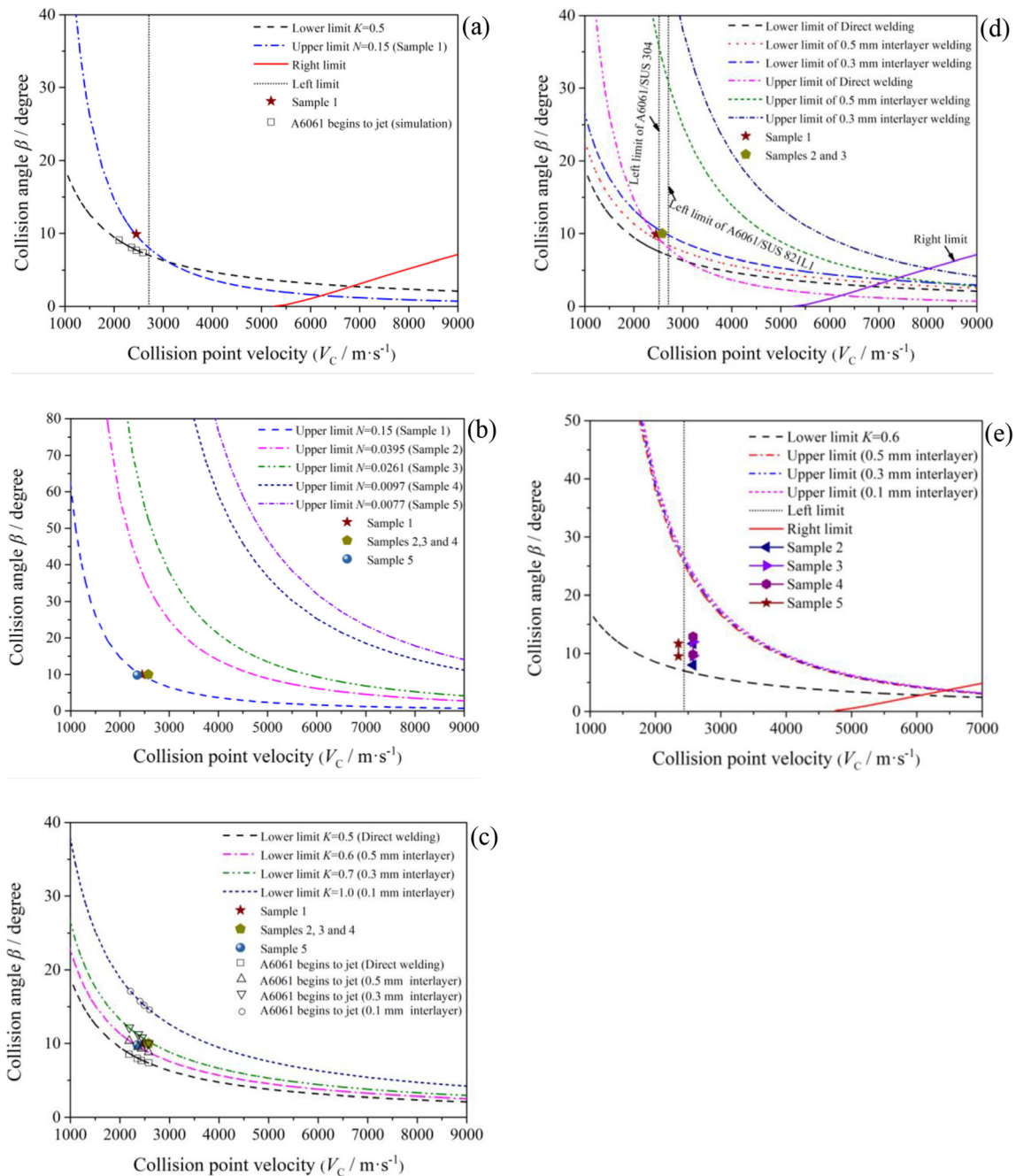**Table 11** Collision angle between the interlayer and the base plate

Samples	Collision angle β_{2min}	Collision angle β_{2max}
2	8.0°	11.7°
3	9.6°	12.0°
4	9.8°	12.9°
5	9.5°	11.7°

between A6061 and interlayer was 208.6 MPa; the fracture appeared on the interface between A6061 and interlayer. When the thickness of the interlayer was 0.1 mm, the welding could not be achieved, due to the low energy deposited on the interface.

2. The pressure peak of air shock between plates was calculated and simulated. The simulation results are in accordance with the calculation results. When the detonation velocity was 2450 m/s, the pressure peak of air shock wave was 8.676 MPa (calculation results); when the

Table 12 Properties of TP 270C, SUS 821L1, and SUS 304 [13, 23, 30]

	Density ρ (kg·m^{-3})	Melting temperature T_m (°C)	Bulk sound speed C_b (m·s^{-1})	Thermal conductivity λ (W·m^{-1}·K^{-1})	Specific heat C_p (J·kg^{-1}·K^{-1})
A6061	2700	585	5240	167.0	897
SUS821L1	7800	1400	4569	16.0	500
SUS304	7930	1400	4569	16.3	500

Fig. 10 Weldability window **a** direct welding of A 6061/SUS 821L1; **b** upper limits for A 6061/SUS 304 using different interlayers; **c** lower limits for A 6061/SUS 304 using different interlayers; **d** comparison of direct welding and interlayer welding; **e** window between the interlayer and the base plate

detonation velocity was 2575 m/s, the pressure peak of air shock was 10.417 MPa (calculation results). Through theoretical and numerical simulation analysis, it was demonstrated the air shock wave between the plates affected the movement of the interlayer during the process of explosive welding. The effect of air shock wave on 0.1-mm interlayer was more pronounced than that of 0.8-mm interlayer. The air shock wave had a negative effect on the welding results, particularly for large plates.

3. The variation trend of interfacial jet and melting obtained by simulation was consistent with the experimental results. The simulation results showed the welding failure of direct welding was due to excessive melting of A6061; the welding failure of 0.1-mm interlayer was due to the unmelted A6061. The collision angle between interlayer and base plate was estimated using numerical simulation.

4. The interlayer led to an upward shift of the upper and lower limits of the weldability window, the area of the window expanded, and the range of the possible welding parameters expanded, facilitating welding. The parameter K in the lower limit of the weldability window was obtained using numerical simulation. The K of direct welding was 0.5; the K of 0.5-mm interlayer welding was 0.6; the K of 0.3-mm interlayer welding was 0.7; the K of 0.1-mm interlayer welding was 1.0.

Data availability Not applicable.

Code availability Not applicable.

Declarations

Ethics approval Not applicable.

Consent to participate All authors have approved to participate.

Consent for publication The manuscript is approved by all authors for publication.

Conflict of interest The authors declare no competing interests.

References

1. Hatano R, Ogura T, Matsuda T, Sano T, Hirose A (2018) Relationship between intermetallic compound layer thickness with deviation and interfacial strength for dissimilar joints of aluminum alloy and stainless steel. Mat Sci Eng A-Struct 735:361–366. https://doi.org/10.1016/j.msea.2018.08.065

2. Ogawa D, Kakiuchi T, Hashiba K, Uematsu Y (2019) Residual stress measurement of Al/steel dissimilar friction stir weld. Sci Technol Weld Join 24(8):685–694. https://doi.org/10.1080/13621718.2019.1588521

3. Nguyen VN, Nguyen QM, Huang SC (2018) Microstructure and mechanical properties of butt joints between stainless steel SUS304L and aluminum alloy A6061-T6 by TIG welding. Materials 11(7):1136. https://doi.org/10.3390/ma11071136

4. Liu S, Suzumura A, Ikeshoji TT, Yamazaki T (2005) Brazing of stainless steel to various aluminum alloys in air. JSME Int J A-Solid M 48(4):420–425. https://doi.org/10.1299/jsmea.48.420

5. Sherpa BB, Kumar PD, Upadhyay A, Kumar S, Agarwal A, Tyagi S (2021) Effect of explosive welding parameters on Al/LCS interface cladded by low velocity of detonation explosive welding (LVEW) process. Int J Adv Manuf Technol 113(11):3303–3317. https://doi.org/10.1007/s00170-021-06800-5

6. Malakhov A, Saikov I, Denisov I (2021) Brass/Invar bimetal by explosive welding. Int J Adv Manuf Technol 114(1):357–364. https://doi.org/10.1007/s00170-021-06897-8

7. Yang M, Ma H, Shen Z (2018) Study on self-restrained explosive welding with high energy efficiency. Int J Adv Manuf Technol 99(9):3123–3132. https://doi.org/10.1007/s00170-018-2600-y

8. Carvalho G, Galvão I, Mendes R, Leal R, Loureiro A (2018) Explosive welding of aluminium to stainless steel. J Mater Process Technol 262:340–349. https://doi.org/10.1016/j.jmatprotec.2018.06.042

9. Hokamoto K, Izuma T, Fujita M (1993) New explosive welding technique to weld. Metall Mater Trans A 24(10):2289–2297. https://doi.org/10.1007/BF02648602

10. Miao Y, Chen X, Wang H (2021) Some applications of interlayer explosive welding. Compos Interface:1–16. https://doi.org/10.1080/09276440.2021.1943142

11. Han JH, Ahn JP, Shin MC (2003) Effect of interlayer thickness on shear deformation behavior of AA5083 aluminum alloy/SS41 steel plates manufactured by explosive welding. J Mater Sci 2003 38(1):13–18. https://doi.org/10.1023/A:1021197328946

12. Carvalho G, Galvão I, Mendes R, Leal R, Loureiro A (2020) Explosive welding of aluminium to stainless steel using carbon steel and niobium interlayers. J Mater Process Technol 2020(283):116707. https://doi.org/10.1016/j.jmatprotec.2020.116707

13. Chen X, Inao D, Tanaka S, Mori A, Li X, Hokamoto K (2020) Explosive welding of Al alloys and high strength duplex stainless steel by controlling energetic conditions. J Manuf Process 58:1318–1333. https://doi.org/10.1016/j.jmapro.2020.09.03714

14. SUS304 Stainless steel material properties, chemical composition, meaning. (2021) The world material. https://www.theworldmaterial.com/sus304-stainless-steel-material/. Accessed 2 July 2021.

15. Duplex stainless steel. (2021) UEX,LTD. https://www.uexltd.co.jp/english/products/nisou_stainless/. Accessed 2 July 2021.

16. Aluminum vs. 5052 aluminum - differences in properties, strength and uses (2021) Thomas. https://www.thomasnet.com/articles/metals-metal-products/6061-aluminum-vs-5052-aluminum/. Accessed 2 July 2021.

17. Sakai Y (2012) Success with new products. https://www.metalbulletin.com/events/download.ashx/document/speaker/6540/a0ID000000X0jUf MAJ/Presentation. Accessed 20 April 2021.

18. Manikandan P, Hokamoto K, Deribas AA, Raghukandan K, Tomoshige R (2006) Explosive welding of titanium/stainless steel by controlling energetic conditions. Mater Trans 47(8):2049–2055. https://doi.org/10.2320/matertrans.47.2049

19. Crossland B (1982) Explosive welding of metals and its application. Clarendon Press • Oxford.

20. Deribas A (2001) Science of explosive welding: state of art. In Impact Engineering and Application, Proceeedings of the 4th International Symposium on Impact Engineering, Chiba, A.; Tanimura, S.; Hokamoto, K., Eds. ELSEVIER. 530-531.

21. Tanguay V, Higgins A (2004) The channel effect: coupling of the detonation and the precursor shock wave by precompression of the explosive. J Appl Phys 96(9):4894–4902. https://doi.org/10.1063/1.1787913

22. Taylor WC, Chown JB, Morita T (1968) Measurement of rf ionization rates in high- temperature air. J Appl Phys 39(1):191–194. https://doi.org/10.1063/1.1655730

23. Johnson G, Cook W (1969) Selected hugoniots: EOS. In 7th International Symposium on Ballistics. LA-4167-MS.

24. Yang X, Ling X, Zhou J (2014) Optimization of the fatigue resistance of AISI304 stainless steel by ultrasonic impact treatment. Int J Fatigue 61:28–38. https://doi.org/10.1016/j.ijfatigue.2013.12.003

25. Akram S, Jaffery SHI, Khan M, Fahad M, Mubashar A, Ali L (2018) Numerical and experimental investigation of Johnson–Cook material models for aluminum (Al 6061-T6) alloy using orthogonal machining approach. Adv Mech Eng 10(9):1687814018797794. https://doi.org/10.1177/1687814018797794

26. Mahmood Y, Guo B, Chen P, Zhou Q, Bhatti A (2020) Numerical study of an interlayer effect on explosively welded joints. Int J Multiphysics 14(1):69–80. https://doi.org/10.21152/1750-9548.14.1.69

27. Aizawa Y, Nishiwaki J, Harada Y, Muraishi S, Kumai S (2016) Experimental and numerical analysis of the formation behavior of intermediate layers at explosive welded Al/Fe joint interfaces. J Manuf Process 24:100–106. https://doi.org/10.1016/j.jmapro.2016.08.002

28. Zeng X, Li X, Li X, Mo F, Yan H (2019) Numerical study on the effect of thermal conduction on explosive welding interface. Int J Adv Manuf Technol 104(5):2607–2617. https://doi.org/10.1007/s00170-019-04054-w

29. Chen X, Li X, Wang X, Yan H, Li K, Zeng X (2019) Bonding mechanism of explosive compaction–welding sintering. J Manuf Process 46:1–15. https://doi.org/10.1016/j.jmapro.2019.08.018

30. Okada N, Tadokoro Y, Tsuge S, Gonome F, Kizaki M (2017) Lean duplex stainless steel for resources saving society. Zairyo-to-Kankyo 66(8):263–267. https://doi.org/10.3323/jcorr.66.263

31. Cowan G, Bergmann O, Holtzman A (1971) Mechanism of bond zone wave formation in explosion-clad metals. Metall Mater Trans B Process Metall Mater Process Sci 2(11):3145–3155. https://doi.org/10.1007/BF02814967

32.] De Rosset (2006) Analysis of explosive bonding parameters. Mater Manuf Process 21 (6): 634-638. https://doi.org/10.1080/10426910600611136